Naseema K.*, Rakhi Sreedharan, Sarath Ravi, Raghi K. R. and Manoj Kumar T. K.

Experimental and computational studies on optical properties of a promising N-benzylideneaniline derivative for non-linear optical applications

https://doi.org/10.1515/zna-2020-0047 Received February 17, 2020; accepted April 6, 2020; published online May 11, 2020

Abstract: A new organic non-centrosymmetric nonlinear optical (NLO) material, p-nitrobenzylidene-p-phenylamineaniline (PNBPDA) was synthesized and single crystals of PNBPDA were grown from ethanol solution by slow evaporation solution growth technique. Single crystal Xray diffraction (XRD) and powder XRD data confirm that PNBPDA crystallizes in monoclinic system with noncentrosymmetric space group Cc. Various characterizations like PXRD, fourier transform infrared (FT-IR) spectroscopy, thermal analysis and micro hardness test have been conducted. Optical studies have been done for evaluating the transparency range and the luminescence property of the grown single crystals of PNBPDA. Dielectric studies have carried out to investigate the electronic polarizability within the grown crystal. The frequency conversion efficiency of the grown crystal was determined using Kurtz Perry powder technique and second harmonic generation (SHG) was found to be 6 times that of standard Potassium Dihydrogen Phosphate (KDP). Z-Scan technique was performed to determine the third order non-linear optical properties of the grown crystal of PNBPDA. The optical limiting property and the laser damage threshold value reflect the practical applicability of PNBPDA crystal for photonic applications. Additionally, the theoretical background of PNBPDA was carved out using Density Functional Theory (DFT) by evaluating the geometrical and electronic structural properties from Frontier Molecular Orbital (FMO) analysis, Molecular Electrostatic Potential (MESP) analysis and non-linear features from dipole moment, polarizability and hyperpolarizability properties embedded within the PNBPDA molecule. The calculated first order hyperpolarizability (β) value of the molecule was found to be 14 times that of the standard urea molecule.

Keywords: linear and non-linear optical studies; optical limiting applications; organic NLO crystal; quantum chemistry calculations; synthesis and growth.

1 Introduction

Non-linear optical (NLO) materials have acquired wide acceptance by the past two decades due to their potential applications in the fields of optical telecommunication, optical computing, optical information processing and high optical disk data storage [1–4]. The most prominent property that every NLO material should possess was its challenging optical transparency throughout the UVvisible region with less deformations and dislocations within the lattice sites of the material [5]. Among the NLO materials, organic materials have been reported to be a promising aspirant because of their enhanced molecular nonlinearity over a broad frequency range, less optical absorption, high thermal stability and adequate mechanical strength which can be exploited in optoelectronic and photonic applications [6, 7]. Within the organic NLO material category, N-benzylideneaniline derivatives play an excellent role among the organic category due to the presence of delocalized π electron conjugated groups arranged without a chiral centre in the lattice and hence results in an increase in the hyperpolarizability values which can pave the way for far better NLO responses.

The crystal structures of three new organic compounds of N-benzylideneaniline derivatives such as p-nitro-benzylidene-p-phenylamineaniline, 2,4-dinitrobenzylidene-p-dieth-ylamineaniline and p-dinitrobenzylidene-p-dieth-ylamineaniline containing electron-push-pull groups with non-centrosymmetric crystal packing, a significant

^{*}Corresponding author: Naseema K., Department of physics, Nehru Arts and Science College, Kanhangad, 671314, Kerala, India, E-mail: nascrakhi@gmail.com

Rakhi Sreedharan and Sarath Ravi: School of Pure and Applied Physics, Payyanur Campus, Kannur University, Kannur, 670327, Kerala, India

Raghi K. R. and Manoj Kumar T. K.: School of Chemical Sciences, Payyanur Campus, Kannur University, Kannur, 670327, Kerala, India; Indian Institute of Information Technology and Management, Trivandrum, 695581, Kerala, India

property for non-linear behaviour, have been reported [8]. In this submission we investigate the various chemical, physical linear and non-linear optical characterization of p-nitrobenzylidene-p-phenylamineaniline ($C_{19}H_{15}N_3O_2$), which remains unexplored till now. In the titular compound, phenylamine act as the electron donating group and the nitro group at the fourth position of benzylidene act as the electron withdrawing group where the neighboring functional groups are linked with the N-benzylidene core through an efficient intermolecular charge transfer (CT) [8]. Along with the experimental data, some theoretical investigations of p-nitrobenzylidene-p-phenylamineaniline (PNBPDA) molecule (Figure 1) have also been included using Density Function theory formalism which strongly agrees with that of the experimental findings.

2 Experimental procedure

2.1 Material synthesis

All the reagents of n-phenyl-p-phenylenediamine and p-nitrobenzaldehyde required for synthesizing PNBPDA compound was purchased from sigma Aldrich and used without further purification. The saturated solution of the deep-red mixture of n-phenyl-p-phenylenediamine (184.2 mg, 1.001 mmol) and p-nitrobenzaldehyde (151.2 mg, 1.001 mmol) prepared in adequate quantity of ethanol has undergone vigorous stirring for about 6 h at room temperature to obtain a homogeneous solution of the resultant compound. The solvent was removed incorporating rotary evaporation and the obtained precipitate was again dissolved in chloroform for the crystallization process. Then the obtained solution was filtered off using Whatmann

filter paper (Grade I) and kept in a dust free atmosphere for evaporation. Small red coloured prismatic shaped seed crystals of p-nitrobenzylidene-p-phenylamineaniline were observed within two weeks after successive recrystallization using methanol and chloroform.

2.2 Solubility of the material

After the synthesis of the title compound, the solubility was determined in the temperature range of 30 °C to 65 °C by maintaining the solution in a temperature controlled water bath of ± 0.01 °C. The recrystallized sample of PNBPDA was first dissolved in 100 ml of ethanol and water by continuous stirring at 30 °C and the resultant homogeneous saturated solution was filtered. About 5 ml of the solution was pipetted out to a petri dish and the amount of solvent present in the solution was calibrated gravimetrically. From the data, the accurate quantity of PNBPDA sample dissolved in 100 ml of the two solvents at 30 °C was determined. The procedure was repeated for 35, 40, 45, 50, 55, 60 and 65 °C and the corresponding amount of PNBPDA dissolved at respective temperatures was noted. The variation in solubility for two solvents as a function of temperature is portrayed in Figure 2a. In accordance with the solubility data, we inferred that the material holds a positive temperature co-efficient exhibiting an increasing variation in solubility of PNBPDA with an increase in temperature.

2.3 Crystal growth

The obtained red prismatic seed crystals via re-crystallization using the mixture of methanol and chloroform were

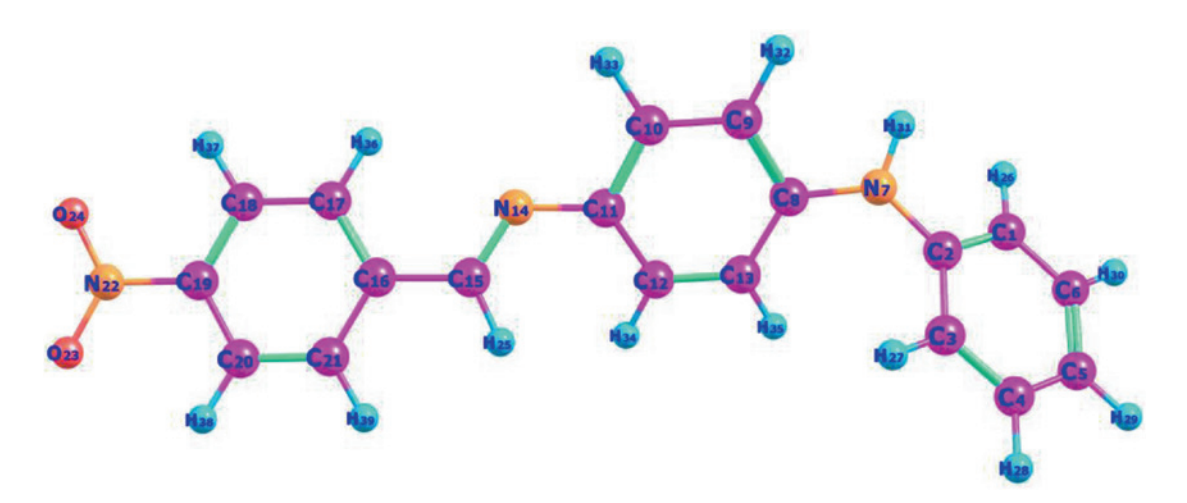
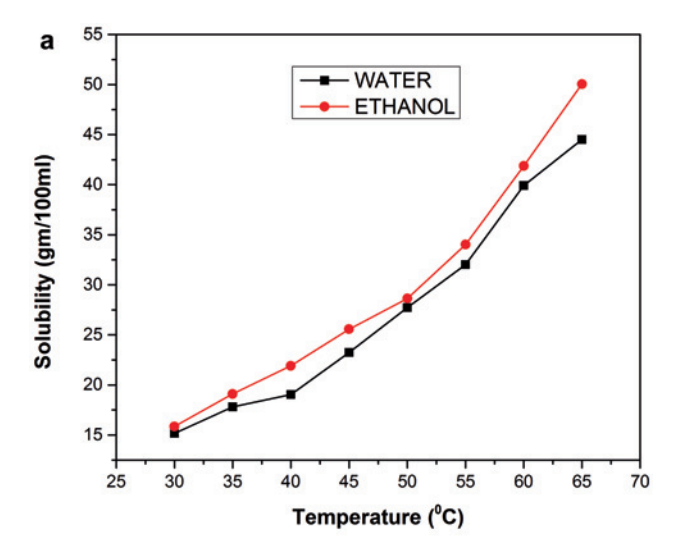


Figure 1: 2D molecular structure of PNBPDA.



b

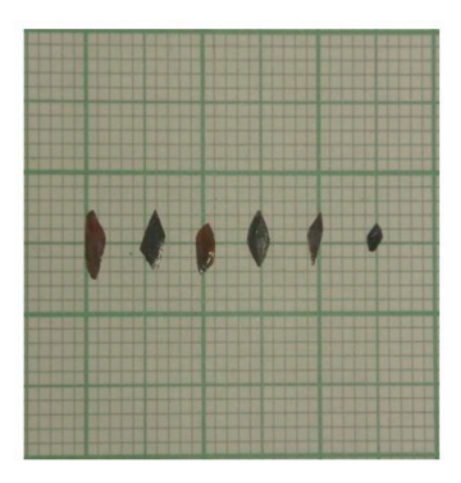


Figure 2: (a) Solubility data of PNBPDA crystal (b) Grown single crystals of PNBPDA.

successfully grown by the conventional slow evaporation solution growth technique using ethanol as the solvent. For the growth of bulk single crystals of PNBPDA, the recrystallized red prismatic seed crystals were dissolved in ethanol by maintaining a temperature of 30 °C. The obtained saturated homogeneous solution was filtered and covered using perforated polythene sheet for ensuring the controlled slow evaporation process. Thus bulk crystals of PNBPDA of prismatic shape with significant dimension were harvested within a period of one week and it was then used for further investigations. The obtained red prismatic single crystal was as shown in Figure 2b.

2.4 Characterization techniques

Single crystal X-ray diffraction (XRD) analysis was performed using ENRAF NONIUS CAD4 diffractometer for identifying the cell parameters and Powder X-ray diffraction (PXRD) spectrum was recorded via Cary 630 with ATR- Agilent technologies to confirm the crystalline nature of the obtained PNBDPA single crystal. Fourier Transform Infrared spectrum (FTIR) was examined through Rigaku Miniflex 600 set-up for determining the various functional groups present in the grown crystal. Thermo gravimetric and Differential Scanning Calorimetric (TG&DSC) curves were generated by employing NETZSCH STA 449F5 STA449FSA-0231-M thermal analysis system to examine the thermal stability of the material. Ultra-violet-visible-near infra-red (UV-Vis-NIR) and fluorescence spectra were found by Varian Carry 5000 spectrophotometer and Shimadzu Spectrofluorophotometer respectively to detect the optical transparency and luminescence behaviour of the grown crystal. LEITZ WETZLER micro hardness tester with diamond indenter was used to confirm the mechanical stability of the material, dielectric studies were performed by HIOKI 3532 LCR HITESTER set-up and the second and third order non-linear property of the material was evaluated and confirmed using Kurtz Perry powder technique and Z-Scan technique.

2.5 Quantum computational calculations

The PNBPDA molecule was subjected to computational studies to investigate various electronic and molecular structural parameters as well as the non-linear optical properties to check the practical applicability of the material for various optoelectronic applications. The study was performed choosing hybrid functional density theory with Lee-Yang-Parr correlation density functional (B3LYP: Becke-3-Lee-Yang-Parr) and ab initio time dependent Hartree-Fock (TD-HF) with $6-31++G^*d(p)$ basis set. The optimization of molecule to

ground state (GS) equilibrium geometry, calculation of various structural properties like Frontier Molecular Orbital (FMO) analysis, molecular electrostatic potential analysis and non-linear optical parameters like dipole moment, polarizability and hyperpolarizability were executed at B3LYP method utilizing Gaussian 09 W quantum chemistry package as the software program. The 2D structure of the title compound obtained from the Crystallograhic Information File (CIF) of the reported literature was used for the optimization of the molecular geometry of PNBPDA.

3 Results and discussion

3.1 Crystallographic studies

The grown single crystals of PNBPDA ($C_{19}H_{15}N_3O_2$) were subjected to XRD studies to determine the lattice parameters and the crystal structure of the obtained compound. The result was analysed using ENRAF NONIUS CAD-4 diffractometer. The diffractogram spots represent the intensities corresponding to the X-rays reflected from the lattice site of the crystal [9]. It was found that the crystal crystallizes in the monoclinic system with non-centrosymmetric space group Cc. The obtained data via X-ray diffractometer was verified with the already reported details and a comparative study was shown in the Table 1 as below;

Powder XRD analysis has been carried out to identify the crystallinity and the purity of the grown PNBDPA single crystals. The sample was scanned over the angular range of 5° – 70° with a step increment of 0.02° using CuK α (λ = 1.5148A°) radiation and Bragg's peaks corresponding to particular 2θ angle was plotted (Figure 3). The existence of sharp Bragg's peaks at specific 2θ angle confirms the crystalline nature of the obtained compound.

Table 1: Comparison of the unit cell parameters of PNBPDA crystal with the reported values.

Crystal data	Present study	Reported [8]
a(A)	10.64	10.3885
b(A)	17.10	16.7902
c(A°)	8.98	8.9064
α (degree)	90.00	90.00
β (degree)	98.02	97.704
Y (degree)	90.00	90.00
Cell volume ((A)3)	1619	1539.48
Crystal system	Monoclinic	monoclinic
Space group	Сс	Сс

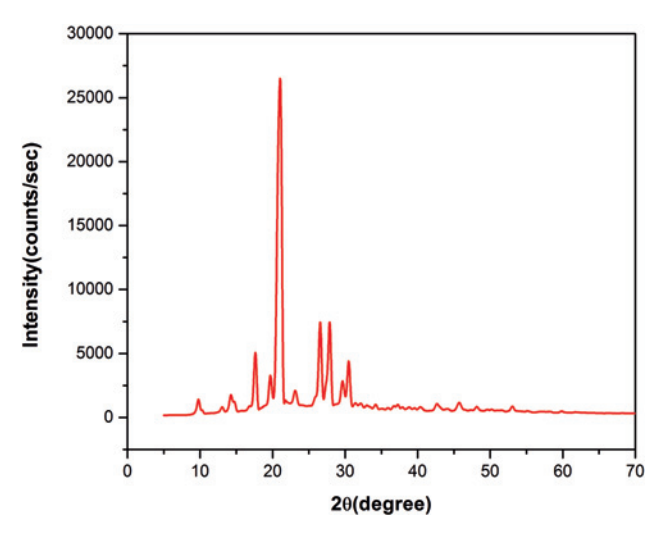


Figure 3: Powder XRD spectrum of PNBPDA single crystal.

Powder XRD analysis helps us to determine the crystalline nature of the grown crystal by exploiting various parameters like crystallite size, degree of crystallinity, dislocation density and the effect of microstrain within the grown crystal of PNBPDA.

The crystallite size of PNBPDA was evaluated using Debye–Scherrer's formula;

$$D = \frac{k\lambda}{\beta\cos\theta} \tag{1}$$

where k = 0.9, $\lambda = 1.5405$ A° & β corresponds to the peak width of the reflection at half intensity. Here the maximum intensity was observed to be at $2\theta = 21.029^\circ$. Hence the size of the crystal was found to be 142 A°. This was then verified from the Hall Williamson plot which is depicted in figure. The dislocation density of the crystal lattice was determined via the relation;

$$\delta = \frac{1}{D^2} \tag{2}$$

The presence of microstrain with the lattice was obtained using the Hall Williamson equation;

$$\varepsilon = \frac{1}{Sin\theta} \left[\beta \cos \theta - \frac{\lambda}{D} \right] \tag{3}$$

It was also in good agreement with the slope of the linear fitted region from the Hall-Williamson plot (Figure 4) [10]. The crystalline nature of the grown crystal was then strictly confirmed by calculating the percentage of crystallinity embedded within the PNBPDA sample.

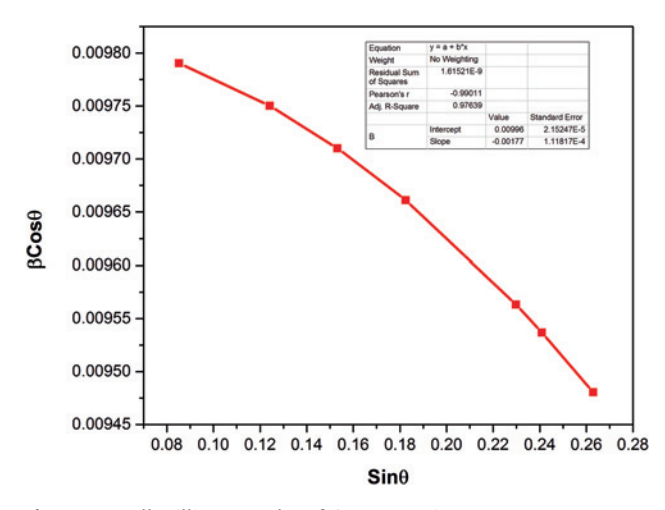


Figure 4: Hall Williamson Plot of β Cos θ Vs Sin θ .

The determined structural parameters are tabulated in Table 2.

3.2 FTIR analysis

In vibrational spectroscopy, various functional groups present within a material would be identified by observing the absorption spectral bands recorded in the FTIR. Depending on the nature of the material, distinct frequencies will be absorbed by different functional groups for carrying out the stretching, wagging, bending and rocking vibrations within the material. The various functional groups and the corresponding vibrational assignments will provide us limited information about the molecules present within the obtained compound. Here the vibrational spectrum was recorded at room temperature in the range of 4000 cm⁻¹ to 500 cm⁻¹ using KBr beam splitter with a He-Ne laser source. In the observed FTIR spectrum (Figure 5), a sharp band identified at 3406 cm⁻¹ could be attributed to N-H asymmetric stretching and 2873 cm⁻¹

Table 2: Crystallographic parameters of PNBPDA crystal.

Crystallographic parameters	Values
Maximum peak (2θ)	21.029°
FWHM (β)	0.01 (radian)
Crystallite size	
Debye Scherrer equation	142 A°
Hall Williamson plot	100 A°
Dislocation density(δ)	$0.492 \times 10^{12} \text{ g/cm}^3$
$Microstrain(\varepsilon)$	
Hall Williamson equation	-0.005
Hall Williamson plot	-0.002
Degree of Crystallinity	38%

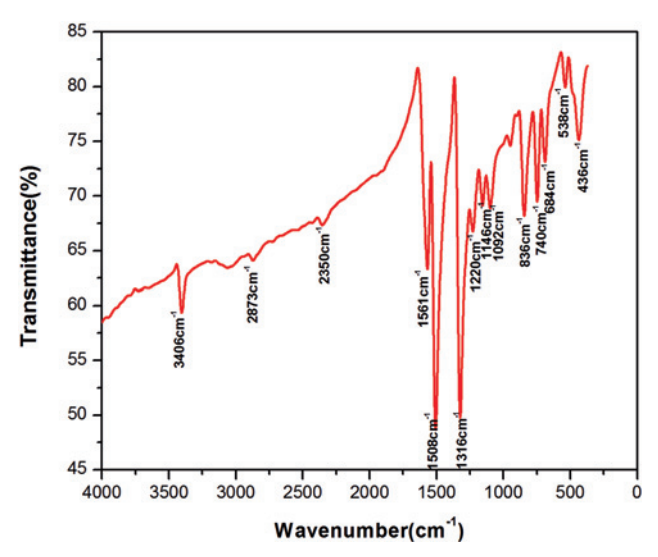


Figure 5: FTIR spectrum of PNBPDA single crystal.

band has been assigned to aromatic C-H asymmetric stretching. A medium weak band occurred at 2350 cm⁻¹ were the characteristic of N-H... O stretching whereas a sharp peak identified at 1561 cm⁻¹ and 1508 cm⁻¹ could be due to the effect of NO2 asymmetric stretching and C=C symmetric stretching. A medium strong band was predicted at 1316 cm⁻¹, 1220 cm⁻¹ and 1146 cm⁻¹ confirmed the occurrence of C-H bending, C-C asymmetric stretching and C-O bending vibrations. At higher frequency ranges, around 1092 cm⁻¹ and 836 cm⁻¹, a sharp intensity peak was appeared and it is contributed by the stretching and bending modes of N-C-N and C-C functional groups. Later on, the rocking of CH₂ group and the out of plane bending vibrations of C-H groups are confirmed by the absorption bands viewed at 740 cm⁻¹ and 684 cm⁻¹. Similarly, the sharp absorption frequencies represented by 538 cm⁻¹ and 436 cm⁻¹ represents the bending vibrations of C-O group and the rocking vibrations of NO₂ group in the compound respectively.

3.3 Thermal exploration

The specimen was subjected for thermal characterization, which provides elaborative information about the suitability of the material for non-linear applications. The thermo gram obtained via thermo gravimetric (TG) and differential scanning calorimetric (DSC) analysis helps us to determine the melting point and the decomposition process involved within the material. The TG/DSC profile was obtained between 35 °C and 500 °C with a heating rate of 10 K/min using Al₂O₃ crucible and the formed pattern was illustrated in Figure 6. From the TG curve, it can be

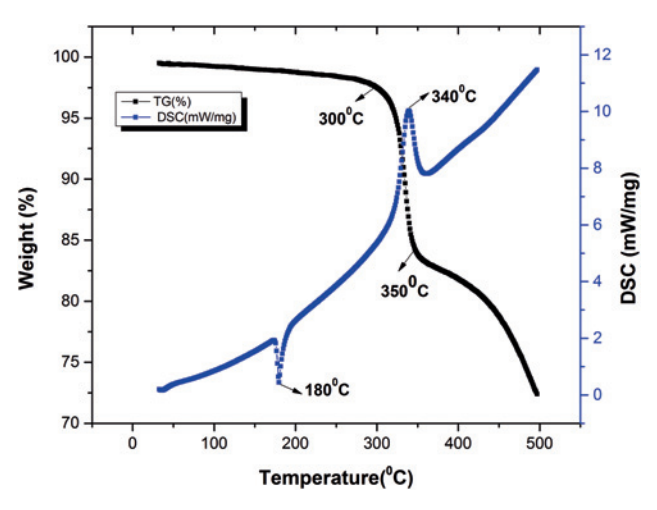


Figure 6: TG/DSC profile of the grown crystal of PNBPDA.

inferred that there is no significant weight loss up to 300 °C which reflects the non-existence of water molecule within the crystal and a major mass loss was observed from 300 °C to 350 °C, which might be due to the liberation of moieties as volatile gaseous products like CO, CO₂, and nitro groups [10]. Hence, the melting temperature of the sample was found to be 300 °C. But in the temperature range 360 °C to 500 °C, there exists a consistent decrease in mass within which the residual product undergoes complete decomposition and the entire mass will be collapsed to zero. DSC profile exhibits a sharp endothermic peak and a sharp exothermic peak at 180 °C and 340 °C respectively and confirms the starting stage of the decomposition of the sample before melting and the exothermic peak which coincides with the TG data reveals the elimination of functional groups which results in the decaying of the compound [11, 12]. The sharpness of the peak and the higher melting point reveals the crystallinity of the material and its suitability for various optoelectronic applications up to 300 °C.

3.4 UV-VIS-NIR spectrum analysis

Optical transmission spectral analysis provides us some basic information about the electronic band structure, localized states and the presence of defects and deformations within the crystal lattice. Such factors strongly influence the optical properties like scattering, transmittance etc. which can adversely affect the practical usability of the material. i. e. crystal with excellent optical transparency and defect free lattice can only be exploited for promising NLO applications [13, 14]. The UV–visible spectrum of the obtained compound was recorded in the

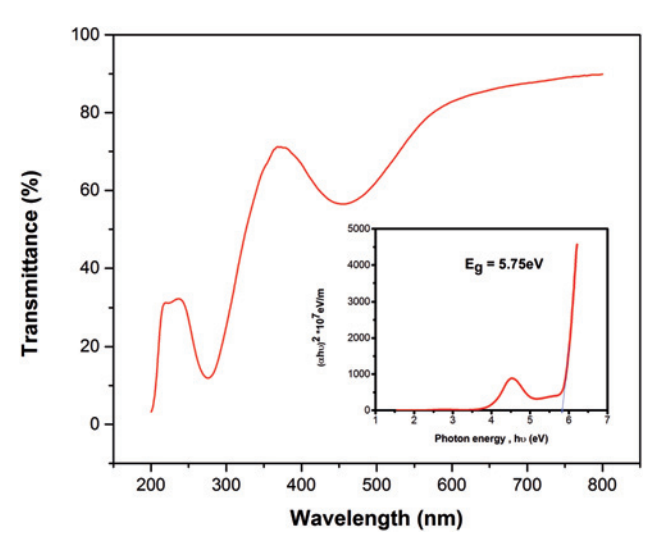


Figure 7: UV-Vis-NIR spectrum of the grown PNBPDA crystal.

wavelength range of 200 to 800 nm and is shown in Figure 7. The spectrum shows significant transmission near the fundamental and second harmonic generation (SHG) signal wavelengths and a small percentage of absorption observed in UV and Visible region could be assigned to the transfer of electrons into the p and *n* orbitals from the GS to the higher excited states [15, 16] and it can be ignored by the prominent transmittance in those region which can confirm the suitability of the material for laser frequency conversion in optoelectronic applications[17].

3.4.1 Determination of optical band gap energy

The optical electronic band gap energy is directly connected to the atomic and electronic band structures, the property that can be well utilized in electro-optical applications [18]. According to Tauc et al., direct band gap energy can be determined by interpreting the expression connecting absorption co-efficient(α) and the obtained transmittance spectrum near the absorption edge as [19];

$$\alpha h \nu = A \mid (h \nu - E_g)^{\frac{1}{n}} \tag{4}$$

The absorption coefficient of any material plays a major role in determining various optical constants like refractive index, optical reflectance, electrical susceptibility and extinction coefficient. Here 'h' is the Planck's constant, ' ν '-frequency of vibration, ' E_g '- optical band gap and 'A''- a proportionality constant. The value of the exponent 'n' denotes the nature of the sample transition [20]. Here n=2 because only the direct allowed sample transition is considered in PNBPDA crystal.

Table 3: Optical parameters of PNBPDA crystal.

Optical parameters	Values
Cut off Wavelength (λ)	276 nm
Band gap energy (E_g)	5.75 eV
Urbach energy (E_u)	1.44 eV
Refractive index (n)	2.31
Optical reflectance (r)	0.157
Electric Susceptibility (χ_c)	4.348

The absorption co-efficient determined from absorption spectra is given by;

$$\alpha = \frac{(2.3036*A)}{t} \tag{5}$$

where'A' is the absorbance and 't' is the thickness of the crystal. The study of optical absorption coefficient with the photon energy helps to understand the type of transition of the electron and the band structure. More effectively the direct optical band gap energy can be graphically obtained by plotting $(\alpha h \nu)^2$ against photon energy $(h \nu)$ and is exhibited in as inset graph of Figure 7. Thus the band gap energy can be accurately found by extrapolating the linear portion of the curve in the Tauc's plot down to the point where $(\alpha h \nu)^2 = 0$ and the value was observed to be 5.75 eV. This higher value of energy recommends the material to be used for UV tunable lasers and NLO device applications [20, 21].

The optical parameters like refractive index of the material(n), optical reflectance(R), electric susceptibility(χ_c) and the Urbach energy(E_{ν}) can be calculated exploiting the following relations and is exhibited in Table 3;

$$n^4 (E_g - 0.365) = 154 (6)$$

$$R = \frac{(n-1)^2}{(n+1)^2} \tag{7}$$

$$\chi_c = n^2 - 1 \tag{8}$$

Urbach rule can be explained as the phenomenon of tailing of the density of states into the forbidden energy gap during the transition of electrons between the top of the valence band to the bottom of the conduction band and the respective Urbach relation is given by:

$$\alpha = \alpha_0 e^{h\nu/E_u} \tag{9}$$

where α_0 – constant, $h\nu$ – photon energy and E_{ν} – Urbach energy.

Urbach energy can be defined as the infinitesimal energy (meV) which reflects the structural disorder within the material encountered by the electrons during transition [23].

Taking logarithm:

$$\ln \alpha = \ln \alpha_0 + \frac{h\theta}{E_u} \tag{10}$$

where E_u is the inverse of the slope of the straight line portion of the graph between $\ln \alpha$ and hv.

3.5 Fluorescence studies

The emission spectrum of an optical material corresponding to a specified excited state helps us to understand the structural arrangement of electrons and its chemical behaviour [24]. The luminescence property will be efficiently shown by compounds having defect free lattices and a prolonged conjugated double bond in aromatic rings [25]. Here the fluorescence spectrum was recorded with the excitation wavelength of 276 nm in the wavelength range of 300 to 360 nm and a high intensity sharp emission was found near 330 nm, which reveals that the grown crystal exhibits UV emission and is illustrated in Figure 8. The band gap energy corresponding to the obtained spectra was then calculated using the expression;

$$E_g = \frac{hc}{\lambda_{\text{max}}} \tag{11}$$

where 'h' is the Planck's constant and 'c', velocity of the light, ' λ_{max} ', the maximum wavelength corresponding to the emission spectrum. Energy gap was determined to be

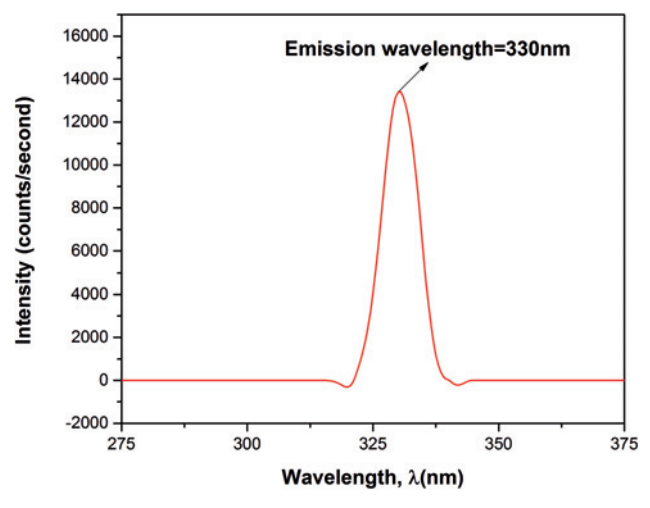


Figure 8: PL emission spectrum of grown PNBPDA single crystal.

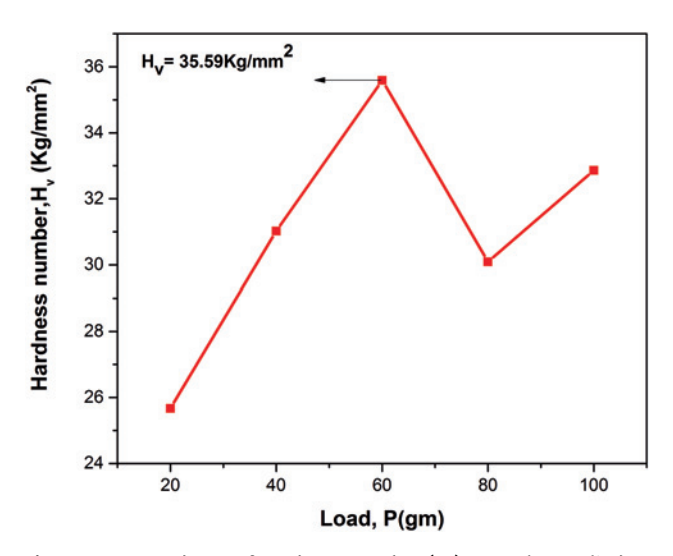


Figure 9: Dependence of Hardness number (H_{V}) upon the applied load (P).

3.76 eV, which demonstrates a decrease in the energy value while emitting the absorbed radiation and is attributed to a significant loss in energy during the electronic transitions.

3.6 Microhardness analysis

The mechanical properties like resistance, brittleness index, stiffness constant and yield strength entangled with hardness of the crystal has to be strictly verified during device fabrications [26]. The hardness of a crystal can be defined as the resistance offered by the material to the localized plastic distortions and deformations arising

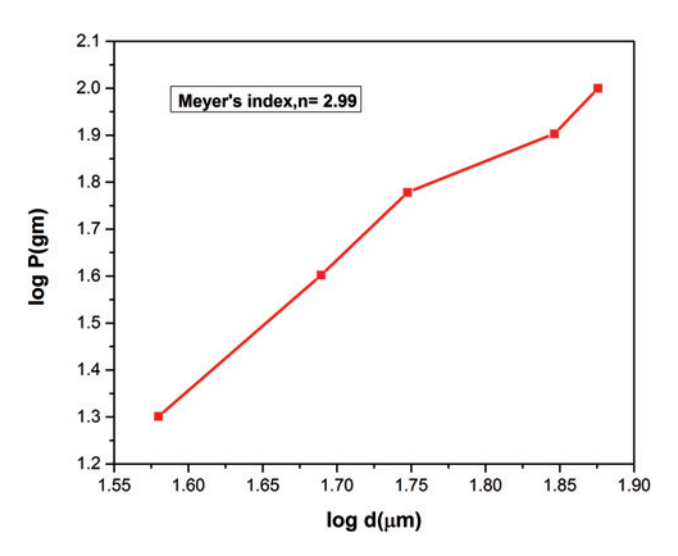


Figure 10: Determination of Meyer's index of the grown PNBPDA crystal.

within the lattice due to the scattering and indentation. Hence the hardness of the material can be found out using Vicker's micro hardness tester by subjecting a well-polished crystal of PNBPDA upon different loads ranging from 20 to 100 gm. The mechanical stability of any material depends on the elasticity of the crystal lattice which would withstand any deformation caused by the impression by producing an internal stress, and this elastic limit can be achieved by a regular packing arrangement of atoms within the crystal lattice which can pave the way for reverse indentation size effect [27]. But beyond an applied load, the elasticity of the material will be lost resulting in the formation of micro cracks within the crystal and this maximum limit up to which a material can withstand stress produced by indentation process is defined as the hardness number related by;

$$H_{\nu} = \frac{1.8544P}{d^2} \tag{12}$$

where ' H_{ν} ' is the Vickers hardness number, 'P' is the applied load in gm and 'd' is the average diagonal length of the indentation marked by the pyramidal indenter in mm. The hardness number of the material with the applied load is graphically shown by Figure 9 (Table 4).

According to Onitsch [28] and Hanneman [29], the applied load (*P*) and the diagonal length of indentation (*d*) is linked by the relation;

$$P = ad^{n} (13)$$

where 'a' is the proportionality constant and 'n' is the Mayer's index number. The above equation can be significantly rearranged as;

$$Log P = Log a + n Log d$$
 (14)

Meyer's index number 'n' can be determined from the graph plotted between 'Log P' on y-axis and 'Log d' in μ m on x-axis as shown in Figure 10. The slope of the graph was found as the Meyer's index number 'n' and was calculated to be 2.99 which is greater than 2, satisfying Onitsch concept and thus confirms that the grown crystal of PNBDPA belongs to soft material category.

Table 4: Mechanical parameters of PNBPDA crystal.

Mechanical parameters	Values
Hardness number (H_{ν})	35.59 Kg/mm²
Meyer's index (n)	2.99
Stiffness constant (C_{11})	$5.186 \times 10^2 \text{N/m}$
Yield strength (s_y)	141.433 Kg/mm ²

Mechanical parameters like stiffness constant and yield strength can be determined using the following relations and the variation in those parameters with the applied load is shown in Figure 11a and b.

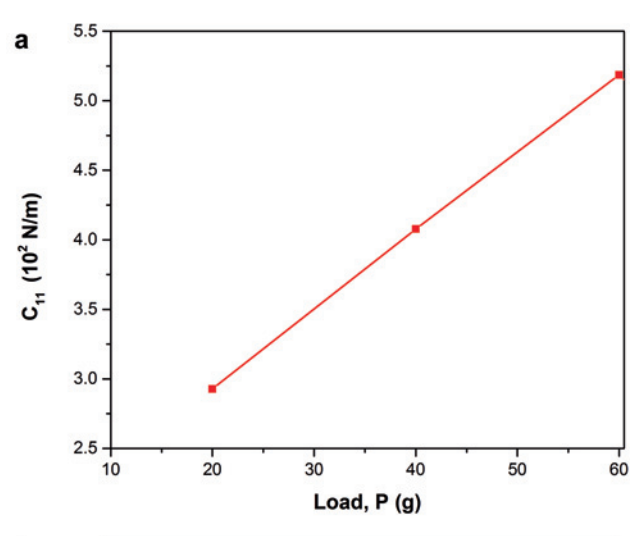
$$C_{11} = (H_{\nu})^{(\bar{\lambda}_{1})} \tag{15}$$

$$\sigma_{y} = \frac{(3-n)}{2.9} \left[\frac{12.5(n-2)}{(3-n)} \right]^{(n-2)} H_{v}, n > 2$$
 (16)

$$\sigma_{y} = \frac{H_{v}}{3}, n < 2 \tag{17}$$

3.7 Dielectric studies

Dielectric property of a material provides some basic knowledge about the lattice dynamics which serves as a



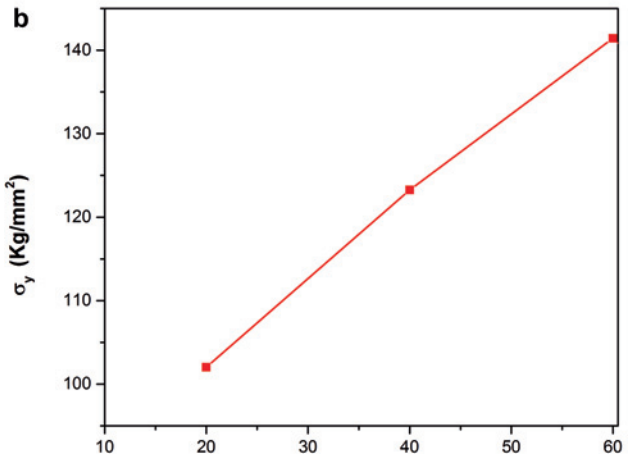


Figure 11: a) Variation of stiffness constant (*C*11). b) Variation of yield strength (σ_v) with the applied load (*P*).

backbone during the fabrication of crystals for non-linear optical applications. It mainly depends on space charge, orientation, ionic and electronic polarization generated due to the electronic displacement occurred within the crystal lattice as a result of the exchange of ions in the crystal for the applied electric field [23, 30].

From the calculated value of parallel capacitance (C_p) , the dielectric constant can be found out using the expression;

$$\varepsilon_r = \frac{C_p d}{\varepsilon_0 A} \tag{18}$$

where d is the thickness of the sample, ε_{0} , the free space permittivity and A describes the area of the sample.

The variation of dielectric constant with that of applied frequency is shown in Figure 12 at three different temperatures (33 °C, 50 °C and 70 °C). Generally, at low frequency region dielectric constant attains a maximum value influenced by space charge polarization and the value eventually got decreased and reaches at a constant with the increase of frequency thereby indicating the occurrence of less energy dissipation as heat [31]. The lower dielectric constant value at high frequency seems to be an admirable property of a material holding defect free lattice and optically good quality crystals, which paves the way for an enhanced NLO behaviour in optical crystals.

3.7.1 Determination of solid state parameters

The electronic polarizability and related parameters can be calculated from the high-frequency dielectric constant (ε_r) and from some crystal sample parameters such as the number of valence electrons (Z) density of the material (ρ) and its molecular weight (M). The valence electron plasma energy is given by;

$$\hbar\omega_p = 28.8\sqrt{\frac{Z\rho}{M}}\tag{19}$$

where Z is the total number of valence electrons, ρ is the density of the PNBPDA sample, M is the molecular mass of the sample, and ω_p is the plasma angular frequency. Here for the PNBPDA crystal, Z value was calculated to be 118, $\rho = 2.316 \text{ g/cm}^3$ and M = 317.34 g/mol.

Hence the Penn gap E_p and Fermi energy E_f can be written as;

$$E_p = \frac{\hbar \omega_p}{\sqrt{(\varepsilon_r - 1)}} \tag{20}$$

$$E_f = 0.2948 \left(\hbar\omega_p\right)^{4/3} \tag{21}$$

Hence the polarizability(α) can be calculated from Penn gap using the following relation;

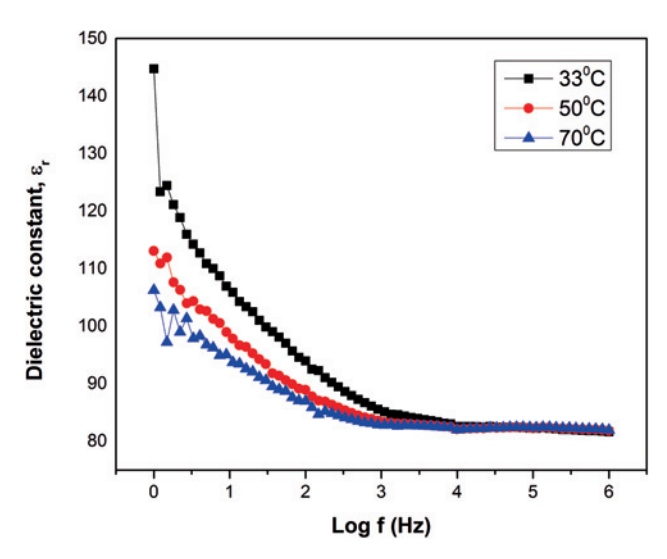


Figure 12: Variation of dielectric constant with the log of the applied frequency.

$$\alpha = \left[\frac{(\hbar \omega_p)^2 S_0}{(\hbar \omega_p)^2 S_0 + 3E_p^2} \right] \frac{M}{\rho} \, \tilde{n} \, 0.396 \, \tilde{n} \, 10^{-24} cm^3 \qquad (22)$$

where S_0 is a constant for the material given by,

$$S_0 = 1 - \left[\frac{E_p}{4E_f}\right] + \frac{1}{3} \left[\frac{E_p}{4E_f}\right]^2$$

The value of the electronic polarizability, α can also be calculated from the Clausius–Mossotti equation, which is given by;

$$\alpha = \frac{3M}{4\pi N_a \rho} \left(\frac{\varepsilon_r - 1}{\varepsilon_r + 2} \right) \tag{23}$$

where N_a is the Avogadro number. The calculated solid state parameters are presented in Table 5 with KDP values for the ease of comparison. The increase in the polarizability values is a good character enhancement for the increase in nonlinear optical properties of the material.

3.8 Laser damage threshold study

While selecting a material for non-linear optical applications in photonic and optoelectronic devices, one must ensure its optical surface damage tolerance or the ability of the material to withstand high power laser beams [32]. For this, Laser Damage Threshold (LDT) study was carried out in order to estimate the stability of

Table 5: Electronic Polarizability parameters of PNBPDA crystal.

Polarizability parameters	Present study	KDP values
Electron plasma energy($\hbar \omega_p$)	26.72 eV	17.33 ev
Penn gap energy (E_p)	2.97 eV	2.39 eV
Fermi energy (E_f)	23.55 eV	12.02 eV
Polarizability (a)	$5.23\times10^{\scriptscriptstyle -23}\text{cm}^{\scriptscriptstyle 3}$	$2.14\times10^{\scriptscriptstyle-23}\text{cm}^{\scriptscriptstyle3}$
(Penn-gap Analysis)		
Polarizability (a)	$5.24\times10^{^{-23}}\text{cm}^{^3}$	$2.18\times10^{^{-23}}\text{cm}^{^3}$
(Clausius – Mosotti equation)		

PNBPDA crystal when subjected to highly intensified laser power. Generally, the threshold value depends on the deformations and defects on the crystal lattice of the grown material which reduces the strength of interatomic bonding between the molecules [33]. The study was performed under Q-Switched Nd-YAG laser source of 532 nm wavelength, pulse width of 9 ns with pulse repetition rate of 10 Hz. The measurement was done on the flat surface of PNBPDA crystal of thickness 0.8 mm by placing the sample at the focal point of the converging lens of focal length, 10 cm. The energy with which crystal got damaged was observed to be at 3.7 mJ/pulse and the radius of the circular spot size was found. The damage threshold value was then computed using the standard power density formula;

$$P_d = \frac{E}{\tau A} \tag{24}$$

where E is the input laser energy in millijoules, τ is the nanosecond pulse width and A is the area of the circular spot (πr^2) impinched on the crystal under study. The evaluated value is compared with some standard values as in Table 6.

The obtained LDT value for PNBPDA crystal is 7.342 GW/cm² which is very much greater than the threshold value of KDP and urea crystals. Thus the present non-linear optical material of PNBPDA crystal confirms its candidature in laser assisted NLO applications.

3.9 Second harmonic generation studies

Kurtz Perry powder technique was explored in order to know the frequency conversion efficiency of the title compound because second harmonic generation (SHG) materials with a good transparency window in the UV–Visible region find better practicability in various non-linear optical fields [8, 32]. In this experimental study, the powdered crystalline sample was packed in a capillary

Table 6: Comparison of LDT values with standard materials.

Compound	LDT (GW/cm²)
PNBPDA	7.342
KDP	0.20
Urea	1.50

tube and exposed to Q-switched Nd-YAG pulsed laser of fundamental wavelength 1064 nm with input laser beam parameters of 0.69 J, 10 Hz, 10 ns as the beam energy, pulse rate and pulse width. Then a frequency doubling output of 532 nm was detected by the photomultiplier diode and the power meter records the energy corresponding to the output pulse and it was found to be 0.18 V for the PNBDPA compound. Here KDP sample is used as the reference material to compare the SHG signals to determine the efficiency of the compound for SHG and the output signal was found to be 30 mV. The level of NLO response is greatly influenced by the structural behaviour of the material which implies that the NLO output can be enhanced by the promising occurrence of CT between the individual reactants involved within the synthesis procedure [35]. The strength of SHG signal was examined to be 6 times higher than that of the standard KDP, which strongly recommends the material to be used as a potential candidate for optoelectronic and photonic applications. The obtained SHG value of PNBPDA crystal was compared with some organic derivatives as exhibited in Table 7 [4, 6, 27, 36, 37].

3.10 Z-Scan measurement

Third order non-linear optical properties of PNBPDA crystal were evaluated employing the most effective and sensitive Z-scan technique proposed by sheik Bahae et al. The analysis was performed using continuous wave Nd-YAG laser with wavelength of 532 nm. For the measurement of non-linear absorption co-efficient by open aperture Z-Scan method, the sample is translated through the region of focus and the intensity corresponding to each z position is recorded using the photo multiplier detector which is placed in the far field and the respective laser beam energy is obtained from the digital power meter. The intensity profile is demonstrated with normalized transmittance as a function of *z* positions. The valley curve obtained via open aperture study reveals the reverse saturable behaviour of the sample which promotes to the optical limiting nature of PNBPDA crystal. The transmission equation of two photon absorption (TPA) process to which the experimental data through open aperture has to be fitted is given by;

Table 7: Comparison of the SHG value of PNBPDA crystal with some reported values.

Some organic compound derivatives	SHG values (as multi- ple of KDP)	
N'-[(Z)-(4-methylphenyl)methylidene]-4- nitrobenzohydrazide	0.50 [4]	
4-Amino-(1-methylphenyl)pyridinium bromide	0.73 [6]	
4-acetylpyridine: 4-aminobenzoicacid	1.39 [26]	
4-Aminopyridinium Trichloro acetate	1.50 [34]	
4- hydroxypiperidin-1-yl)(4-methylphenyl) methanone	1.86 [35]	
p-nitrobenzylidene-p-phenylamineaniline (PNBDPA)	6 [present work]	

$$T(z) = \frac{1}{\sqrt{\pi}q_0(z,0)} \int_{-\infty}^{+\infty} \ln[1 + q_0(z,0)e^{-r^2}]dt$$
 (25)

Where,

$$q_{0}\left(z,t
ight) = rac{eta_{eff}I_{0}\left(t
ight)L_{eff}}{\left(1 + rac{z}{z_{0}^{\prime}}
ight)} \,\&\,L_{eff} = rac{\left(1 - e^{-lpha_{0}l}
ight)}{lpha_{0}}$$

 $\beta_{\rm eff}$ is the TPA co-efficient, I_0 , the peak on axis intensity and z_0 , the Rayleigh wavelength.

The sample had a linear transmission of about 83% at the excitation wavelength and it got reduced to 70% of the laser intensity when PNBPDA sample was placed at the beam focus of Z-Scan. Since the sample had high linear transmission, Two photon absorption process was assumed to be the reason for optical limiting behaviour of the material. But a best fit was obtained only when saturable absorption (SA) was also added as an effect along with multi photon absorption processes like two photon and three photon absorption, for the origin of non-linear properties within crystals. Hence contributions from both, saturation of the ground state (GS) absorption and absorption when excited at resonant wavelengths have to be considered as the predominant reasons for the occurrence of non-linearity within the material [38]. Usually the excited state absorption is encountered by an entity called saturation intensity (I_s) [39].

Therefore an effective intensity dependent non-linear absorption co-efficient ($\alpha(I)$) can be represented as;

$$\alpha(I) = \frac{\alpha_0}{\left(1 + \frac{I}{I_c}\right)} + \beta I \tag{26}$$

where α_0 is the unsaturated linear absorption co-efficient, β , TPA or excited state absorption co-efficient. Thus the non-linear parameters β and I_s can be numerically found out by fitting the experimental open aperture Z-Scan curve

(Figure 13) holding the transmission data with the nonlinear pulse propagation equation;

$$\frac{dI}{dz'} = -\left[\frac{\alpha_0}{\left(1 + \frac{I}{I_s}\right)} + \beta I\right] I \tag{27}$$

where z^{l} indicated the propagation distance within the sample.

The numerically estimated values of β and I_s are 0.7 * 10-11 m/W and $12 * 1012 \text{ W/m}^2$.

Various parameters involved in Z-Scan experiment

- (1) Laser used: Q-Switched Nd YAG laser (Continuum, Minilite)
- (2) Laser beam energy: 100 μJ
- (3) Wavelength: 532 nm (frequency doubled output)
- (4) Pulsewidth: 5 ns
- (5) Pulse Repetition rate used approximately 1 pulse in 5 s
- (6) Focal length of Plano Convex lens used: 6.3 cm
- (7) Focal spot radius: 13 µm
- (8) Cuvette path length: 1 mm

3.10.1 Optical limiting property

One of the most important applications of non-linear optics includes optical limiting characteristics of a material with higher order of non-linearity. It is the efficiency of a material to protect sensitive optical devices and human eves from getting damaged of highly intensified laser light [22]. The optical limiting property mainly arises due to the TPA process or excited state absorption process (Reverse saturable absorption). Optical limiting threshold seems to the characteristic parameter expressing the optical limiting behaviour of a material. The threshold value can be found out from the graph showing transmittance as a function of input fluence exhibited as an inset graph of Figure 13. The optical

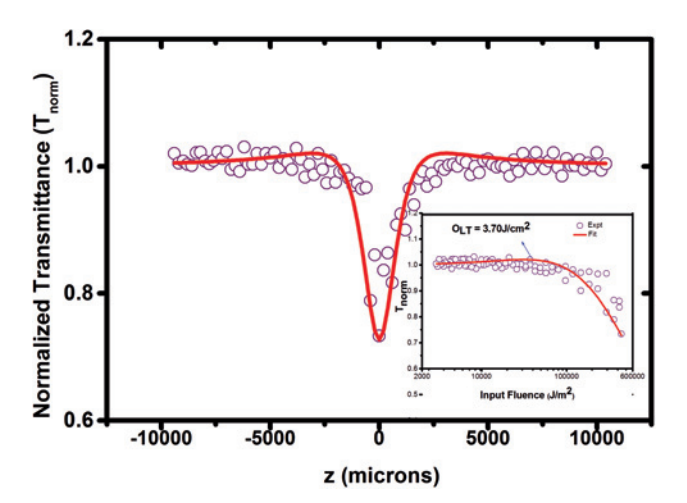


Figure 13: Open aperture Z-Scan curve of PNBPDA crystal.

limiting curve is extracted from the open aperture Z-Scan curve satisfying the equation;

$$I_z = \frac{I_0}{1 + \left(\frac{z^2}{z_0^2}\right)},$$

where $I_0 = \frac{E}{\pi \omega_0^2 \tau}$ and E is the energy of the pulsed laser beam. The low O_{LT} value of PNBPDA sample of 3.70 J/cm² clearly exhibits the good optical limiting character which can be utilized for various photonic applications demanding promising optical limiting performance. The optical limiting values of some organic compounds are gathered in Table 8 for the ease of comparison [1, 22, 40, 41].

3.11 Computed molecular geometry

3.11.1 DFT calculations

The geometry of PNBPDA crystal was optimized by density functional theory (DFT) B3LYP/6-31++ $G \times d(p)$ method using Gaussian 09 W software and visualized by Chemcraft software. FMO energy parameters and Molecular Electrostatic Potential mapping of the PNBPDA were also found out by DFT method with same basis set. Using DFT-B3LYP functions with 6-31 ++ G * d(p) basis set, the most stable structure of the PNBPDA compound was computed and is illustrated in Figure 14a.

3.11.2 Frontier Molecular Orbital (FMO)/HOMO-LUMO analysis

The surfaces of the FMOs were also computed to understand the bonding scheme of PNBPDA and are shown in Figure 14b. From the Figure, the HOMO of the PNBPDA complex is localized over the phenylamine moiety, which primarily acts as an electron donor and the LUMO on the benzylidene moiety, which acts as an electron acceptor. The energies of HOMO (E_{HOMO}) and LUMO (E_{LUMO}) are -5.299 eV and -2.633 eV, respectively. The difference in E_{HOMO} and E_{LUMO} of PNBPDA Compound can be employed to characterize the molecular chemical stability, which is 2.666 eV.

3.11.3 Molecular electrostatic surface potential analysis

For PNBPDA compound, computational DFT/B3LYP approach is used to compute molecular electrostatic potential (MESP) surface. MESP of a compound at a point in space specifies the net electrostatic effect produced at that point, by the total charge distribution of the compound and correlates with partial charges, electronegativity, chemical reactivity and

Table 8: Comparison of O_{LT} values with some organic compound derivatives.

Some organic compound derivatives	Optical limiting threshold value, O_{LT} (J/cm²)
(2E)-1-(Anthracen-9-yl)-3-(4-methox- yphenyl)prop-2-ene-1-one	14.70 [1]
4-dimethylaminopyridinium 3,5-dini- trobenzoate	10.64 [21]
4-methylanilinium 3,5-dinitrobenzoate	7.08 [38]
1,5-Diaminoanthraquinone	5.62 [39]
p-nitrobenzylidene- p -phenylamineaniline	3.70 [present work]

dipole moments of the molecule. Electrostatic potential values are coded with various colours, where red and blue are the most negative and positive regions, and green is the potential neutral region [42]. Simply MESP is the visual method to understand the relative polarity of the molecule. As can be seen from the Figure 14c, more negative potential extended over the amine groups of the phenylenediamine moiety and the positive potential regions are over the nitro groups of the nitrobenzaldehyde moiety.

3.11.4 Dipole, polarizability and hyperpolarizability Calculations

Computational interpretation plays a vital role in determining the molecular structural property relationship which enhances the non-linearity of NLO molecules. The contribution of molecular structure to non-linear behaviour of molecules can be very well explained using some dynamic functions like dipole moment, linear polarizability and hyperpolarizability

on the background of some adequate basis sets like B3LYP and time dependent time dependent Hartree-Fock methods based on finite field approach. The polarizability is recognized to authenticate the ability of an electron cloud to interact with the externally applied electric field which paves the way for an asymmetric distribution of electrons in GS and excited state to increase the optical non-linearity of the molecule. Hyperpolarizability describes the origin of NLO property in system through the occurance of an efficient intermolecular CT interaction within the reactive molecules [29]. One of the most significant key factor describing the non-linearity in the present scenario is the first order hyperpolarizability, a third rank tensor ($3 \times 3 \times 3$ matrices) with 27 components which is later reduced to 10 components by Kleinmann symmetry [43] (Tables 9 and 10). The non-linear optical parameters were then computed by the mathematical formulation of μ , α , β and γ represented as;

Dipole moment,
$$\mu = (\mu_x^2 + \mu_y^2 + \mu_z^2)^{\frac{1}{2}}$$
 (28)

Polarizability,
$$\alpha = \frac{(\alpha_{xx} + \alpha_{yy} + \alpha_{zz})}{3}$$
 (29)

First order hyperpolarizability, $\beta = (\beta_x^2 + \beta_y^2 + \beta_z^2)^{\frac{1}{2}}$ (30)

where
$$\beta_x = \beta_{xxx} + \beta_{xyy} + \beta_{xzz}$$
, $\beta_y = \beta_{yyy} + \beta_{yxx} + \beta_{yzz}$ and $\beta_z = \beta_{zzz} + \beta_{zxx} + \beta_{zyy}$
Second order hyperpolarizability,

$$\gamma = \frac{1}{5} \left(\gamma_{xxxx} + \gamma_{yyyy} + \gamma_{zzzz} + 2\gamma_{xxyy} + 2\gamma_{xxzz} + 2\gamma_{yyzz} \right)$$
 (31)

The dipole moment (u) of PNBPDA crystal was estimated to be 3 times that of the standard reference material

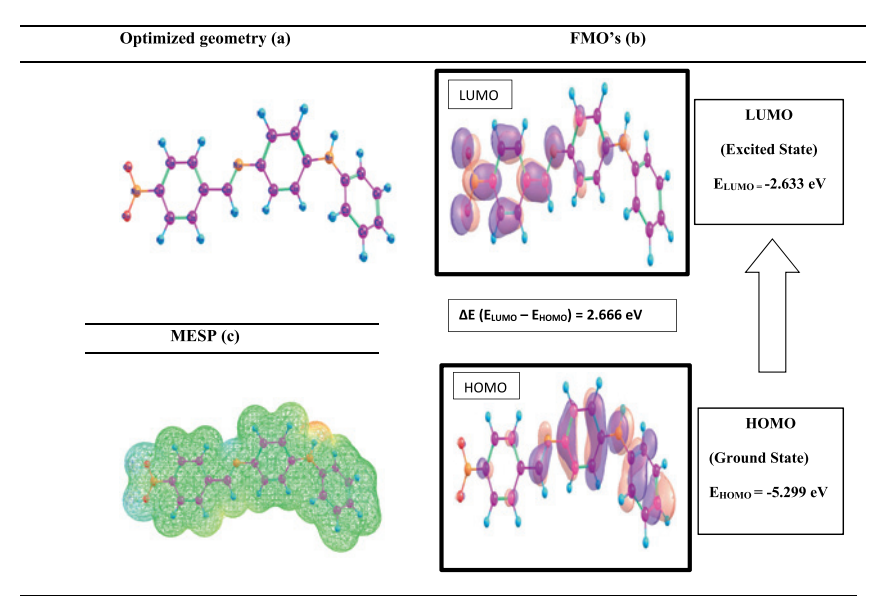


Figure 14: (a) Optimized geometry. (b) FMO analysis. (c) Graphical representation of MESP.

Table 9: Electric dipole moment(μ), linear polarizability(α), first order hyperpolarizability(β) and second order hyperpolarizability(γ) per unit cell volume of PNBPDA molecule.

	B3LYP	Н
Dipole moment (µ	ı) components (Debye, D)	
μ_{x}	7.522	7.089
μ_{y}	-0.067	0.447
μ_{z}	0.155	-0.182
$\mu_{ m total}$ (Debye)	7.523D	7.105
Linear polarizabil	lity (a) components (atomic ui	nit, a.u)
a_{xx}	-176.627	-186.92
a_{yy}	-123.154	-123.689
a_{zz}	-140.135	-144.31
a_{xy}	4.493	-3.97
a_{xz}	-2.641	3.25
a_{vz}	0.131	0.07
α _{total} (a.u)	−146.639 a.u	−151.643 a.
$\alpha_{\rm total}$ (esu)	$-2.2 * 10^{-23}$ esu	-2.275 * 10 ⁻²³ es
irst order hyperp	polarizability (β) components	(atomic unit, a.u)
$oldsymbol{eta}_{xxx}$	639.165	708.65
β_{yyy}	8.221	-7.70
β_{zzz}	-1.119	1.16
β_{xvv}	20.4	20.19
β_{xxy}	40.554	-40.47
$oldsymbol{eta_{xxz}}$	-16.1	21.5
β_{xzz}	-39.252	-41.06
$oldsymbol{eta}_{yzz}$	-0.354	0.64
β_{vvz}	8.416	-10.12
β_{xyz}	-6.439	-7.51
$oldsymbol{eta_{x}}$	620.314	687.79
β_{v}	48.421	-47.53
β_z	-9.703	12.6
β_{total} (a.u)	622.276 a.u	689.547 a.
β_{total} (esu)	5.376 * 10 ⁻³⁰ esu	5.958 * 10 ⁻³⁰ es
-	erpolarizability (γ) componen	nts (atomic unit, a.u)
Yxxxx	-25691.523	-26755.17
γ_{yyyy}	-1202.278	-1191.56
γ _{zzzz}	-230.528	-241.60
γ _{xxxy}	-141.131	183.48
γ _{xxxz}	-319.771	385.18
γ _{yyyx}	46.896	-45.16
γ _{yyyz}	1.136	0.82
γ _{zzzx}	8.567	-7.74
Yzzzy	-1.024	-1.19
Y _{ххуу}	-3624.425	-3665.01
γ _{xxzz}	-3729.701	-3837.23
Yyyzz	-262.203	-267.24
Yxxyz	-54.052	-68.24
γ _{yyxz}	27.703	-32.24
Yzzxy	19.063	-19.73
γ _{total} (a.u)	-8471.398	-8745.46
γ _{total} (esu)	-4.270 * 10 ⁻³⁶ esu	-4.408 * 10 ⁻³⁶ es

of urea (μ = 2.3732D) and the first order hyperpolarizability (β) value was computed to be 14 times that of urea (β = 0.3728 * 10⁻³⁰ esu) which concludes the occurance of CT

Table 10: Non-linear optical parameters obtained from computational analysis.

Non-linear optical parameters	From B3LYP	From HF
Dipole moment (µ)	7.523 debye	7.105 debye
Polarizability (α)	$-2.275 * 10^{-23}$ esu	$-2.2 * 10^{-23}$ esu
First order polarizability (β)	5.376 * 10 ⁻³⁰ esu	5.958 * 10 ⁻³⁰ esu
Second order hyper- polarizability (γ)	-4.270 * 10 ⁻³⁶ esu	-4.408 * 10 ⁻³⁶ esu

interaction within the reactant molecules which plays as the major component for non-linear optical behaviour in materials. The band gap energy of the molecule was calculated to be 2.666 eV. A slight deviation was noticed between the experimentally determined quantities from the theoretical prediction, because computational studies were carried out in gaseous phase whereas experimental characterizations were supported by liquid medium with suitable solvents. Moreover, the experimental results depends on the concentration of solution along with the input laser frequency, intensity of the laser beam, pulse width and the laser repetition rate during the experiment, pulse width, and the intensity of the beam used while performing the experiment whereas the quantum computational studies on non-linearity considers only the given input frequency.

5 Conclusion

The good quality single crystals of an organic NLO material, PNBPDA were grown by the conventional slow evaporation solution growth technique. The cell parameters, purity and the crystallinity of p-nitrobenzylidene-p-phenylamineaniline were confirmed by single crystal XRD and powder XRD data. The functional groups of the PNBPDA crystal were found by FTIR analysis. It was examined that the grown crystal is transparent to all the UV-visible-NIR wavelength range. Hence it can be used for various optoelectronic applications, significantly demanding translucence near IR region. The thermal stability and the mechanical strength of the compound were evaluated via TG/DSC curve and Vicker's micro hardness tester. The electronic polarizability parameters were estimated employing dielectric studies and the laser damage threshold value of the crystal was found to be 7.342 GW/ cm². The Kurtz-Perry powder technique reveals the SHG efficiency of the material as 6 times higher than that of standard KDP, which recommends the suitability of PNBPDA single crystal for laser-assisted non-linear optical applications. Third order non-linear studies were performed using Z-Scan technique for determining the nonlinear absorption co-efficient and saturation intensity. It has ensured the optical limiting nature of PNBPDA crystal with a limiting threshold of 3.70 J/cm². Computational calculations were done for evaluating the HOMO-LUMO energy gap, electrostatic molecular potential mapping and various non-linear optical parameters like dipole moment, polarizability and hyperpolarizability. The first order polarizability was observed to be 14 times that of the standard reference material of urea, which confirms the candidature of PNBPDA crystal for non-linear optical applications. The grown PNBPDA crystal showing excellent stability, purity and enhanced optical activity thus recommends the material to be utilized for photonic and optoelectronic device applications.

Acknowledgement: The authors sincerely thank to Prof. P.K Das, Department of Inorganic chemistry, IISc-Bangalore for extending help to carry out SHG measurement, VIT-Chennai for micro hardness analysis, Saran Raj, Sacred Heart College- Tirupattur for dielectric studies, Priya Dominic and Reji Philip, RRI-Bangalore for providing Z-Scan studies and Nirmalagiri College-Kerala and SAT campus, Kannur University-Kerala for providing various characteristic studies upon the synthesized material.

Conflict of interest: The authors declare that they have no known competing financial interests or personal relationships that could have appeared to influence the work reported in this paper.

References

- [1] S. Ravi, R. Sreedharan, K. R. Raghi, T. K. Manoj Kumar, and K. Naseema, "Experimental and computational perspectives on linear and non-linear optical parameters of an orthorhombic crystal for optical limiting applications," Appl. Phys. A, vol. 126, no. 1, p. 56, Jan. 2020, https://doi.org/10.1007/s00339-019-3234-0.
- [2] D. Yuan, D. Xu, N. Zhang, M. Liu, and M. Jiang, "Organic nonlinear optical crystal MHBA for compact blue-violet laser," Chinese Phys. Lett., vol. 13, no. 11, pp. 841-843, Nov. 1996, https://doi.org/10. 1088/0256-307X/13/11/011.
- [3] M. Iwai, T. Kobayashi, H. Furya, Y. Mori, and T. Sasaki, "Crystal growth and optical characterization of rare-earth (Re) calcium oxyborate ReCa 40(BO 3) 3 (Re = Y or Gd) as new nonlinear optical material," Jpn. J. Appl. Phys., vol. 36, no. 3A, p. L276, 1997.
- [4] K. Naseema, V. Rao, K. V. Sujith, and B. Kalluraya, "Crystal growth and characterization of an NLO organic crystal: N'-[(Z)-(4-methylphenyl) methylidene]-4-nitrobenzohydrazide," Curr. Appl. Phys., vol. 10, no. 4, pp. 1236-1241, Jul. 2010, https://doi.org/10.1016/j.cap.2010.02.050.

- [5] M. Magesh, G. Bhagavannarayana, and P. Ramasamy, "Synthesis, crystal growth and characterization of an organic material: 2-Aminopyridinium succinate succinic acid single crystal," Spectrochim. Acta. Mol. Biomol. Spectrosc., vol. 150, pp. 765-771, Nov. 2015, https://doi.org/10.1016/j.saa.2015.05.
- [6] K. Naseema, V. Rao, K. B. Manjunatha, G. Umesh, K. V. Sujith, and B. Kallurava, "Synthesis, characterization and studies on nonlinear optical parameters of 4-amino-5-(4-nitrophenyl)-1, 2, 4-triazole-3-thione," J. Opt., vol. 39, no. 3, pp. 143-148, Sep. 2010, https://doi.org/10.1007/s12596-010-0006-9.
- [7] K. Naseema, S. Ravi, and R. Sreedharan, "Studies on a novel organic NLO single crystal: L-asparaginium oxalate," Chinese Journal of Physics, vol. 60, pp. 612–622, Aug. 2019, https://doi. org/10.1016/j.cjph.2019.05.037.
- [8] T. E. Souza, I. M. Rosa, A. O. Legndre, et al., "Noncentrosymmetric crystals of new N -benzylideneaniline derivatives as potential materials for non-linear optics," Acta Crystallogr. B Struct. Sci. Cryst. Eng. Mater, vol. 71, no. 4, pp. 416-426, Aug. 2015, https://doi.org/10.1107/ S2052520615008859.
- [9] J. P. Angelena, M. Akilan, K. Raja, J. M. Linet, and S. J. Das, "Growth and characterization of glycinium oxalate crystals in ethanol and methanol," Optik, vol. 126, no. 23, pp. 3912-3916, Dec. 2015, https://doi.org/10.1016/j.ijleo.2015.07.159.
- [10] E. Ilango, R. Rajasekaran, K. Shankar, S. Krishnan, and V. Chithambaram, "Synthesis, growth and characterization of non linear optical Bisthiourea ammonium chloride single crystals by slow evaporation technique," Optic. Mater., vol. 37, pp. 666-670, Nov. 2014, https://doi.org/10.1016/j.optmat. 2014.08.011.
- [11] K. A. Nandekar, J. R. Dontulwar, and W. B. Gurnule, "Thermoanalytical studies and kinetics of newly synthesized copolymer derived from p-hydroxybenzoic acid, and semicarbazide," Rasayan J. Chem., vol. 5, p. 8, 2012.
- [12] R. A. Khatri, S. S. C. Chuang, Y. Soong, and M. Gray, "Thermal and Chemical Stability of Regenerable Solid Amine Sorbent for CO2 Capture," Energy Fuels, vol. 20, no. 4, pp. 1514-1520, Jul. 2006, https://doi.org/10.1021/ef050402y.
- [13] P. R. Deepthi and J. Shanthi, "Optical, dielectric & ferroelectric studies on amino acids doped TGS single crystals," RSC Adv., vol. 6, no. 40, pp. 33686-33694, 2016, https://doi.org/10. 1039/C5RA25700J.
- [14] Ro. Mu. Jauhar, V. Viswanathan, P. Vivek, G. Vinitha, D. Velmurugan, and P. Murugakoothan, "A new organic NLO material isonicotinamidium picrate (ISPA): crystal structure, structural modeling and its physico-chemical properties," RSC Adv., vol. 6, no. 63, pp. 57977-57985, 2016, https://doi.org/10. 1039/C6RA10477K.
- [15] M. Lydia Caroline and S. Vasudevan, "Growth and characterization of l-phenylalanine nitric acid, a new organic nonlinear optical material," Mater. Lett., vol. 63, no. 1, pp. 41–44, Jan. 2009, https://doi.org/10.1016/j.matlet.2008. 08.059.
- [16] M. Prakash, D. Geetha, and M. Lydia Caroline, "Crystal growth, structural, optical, spectral and thermal studies of tris(lphenylalanine)l-phenylalaninium nitrate: A new organic nonlinear optical material," Spectrochim. Acta. Mol. Biomol. Spectrosc., vol. 81, no. 1, pp. 48-52, Oct. 2011, https://doi.org/ 10.1016/j.saa.2011.05.039.

- [17] V. Parol, V. Upadhyaya, G. S. Hegde, N. K. Lokanath, and A. N. Prabhu, "Structural and optical characterization of novel nitro substituted D- π -A- π -A type chalcone single crystal showing second-order and third-order nonlinear optical properties," Physica B: Condens. Matter, vol. 580, p. 411830, Mar. 2020, https://doi.org/10.1016/j.physb.2019.411830.
- [18] V. Krishnakumar, S. Manohar, R. Nagalakshmi, M. Piasecki, I. V. Kityk, and P. Bragiel, "Zinc potassium phosphate hexahydrate crystals for nonlinear optics," Eur. Phys. J. Appl. Phys., vol. 47, no. 3, p. 30701, Sep. 2009, https://doi.org/10.1051/epjap/ 2009094.
- [19] J. Tauc, R. Grigorovici, and A. Vancu, "Optical Properties and Electronic Structure of Amorphous Germanium," Phys. Status Solidi (B), vol. 15, no. 2, pp. 627–637, 1966, https://doi.org/10. 1002/pssb.19660150224.
- [20] C. S. Chandra, Growth, Dislocations and Hardness studies of a nonlinear Optical Crystal- Glycinium Oxalate, vol. 1, p. 5, 2013.
- [21] M. Nageshwari, P. Jayaprakash, C. R. T. Kumari, G. Vinitha, and M. L. Caroline, "Growth, spectral, linear and nonlinear optical characteristics of an efficient semiorganic acentric crystal: Lvalinium L-valine chloride," Physica B: Condens. Matter, vol. 511, pp. 1-9, Apr. 2017, https://doi.org/10.1016/j.physb.2017.01. 027.
- [22] R. Sreedharan, S. Ravi, K. R. Raghi, T. K. M. Kumar, and K. Naseema, "Growth, linear- nonlinear optical studies and quantum chemistry formalism on an organic NLO crystal for optoelectronic applications: experimental and theoretical approach," SN Appl. Sci., vol. 2, no. 4, p. 578, Apr. 2020, https:// doi.org/10.1007/s42452-020-2360-9.
- [23] P. Thomas, R. Junjuri, N. Joy, et al., "Influence of MnCl2 on the properties of an amino acid complex single crystal-l-arginine perchlorate (LAPCI) for optical limiter applications," J. Mater. Sci. Mater. Electron., vol. 30, no. 9, pp. 8407-8421, May 2019, https://doi.org/10.1007/s10854-019-01158-7.
- [24] N. Durairaj, S. Kalainathan, and M. V. Krishnaiah, "Investigation on unidirectional growth of 1.3.5-Triphenvlbenzene by Sankaranarayanan-Ramasamy method and its characterization of lifetime, thermal analysis, hardness and etching studies," Mater. Chem. Phys., vol. 181, pp. 529-537, Sep. 2016, https:// doi.org/10.1016/j.matchemphys.2016.06.090.
- [25] M. S. Kajamuhideen, K. Sethuraman, K. Ramamurthi, and P. Ramasamy, "Crystal growth, physical properties and computational insights of semi-organic non-linear optical crystal diphenylguanidinium perchlorate grown by conventional solvent evaporation method," J. Cryst. Growth, vol. 483, pp. 16-25, Feb. 2018, https://doi.org/10.1016/j.jcrysgro.2017.11.007.
- [26] B. W. Mott, Micro-Indentation Hardness Testing, London, Butterworths, 1956.
- [27] S. Panchapakesan, K. Subramani, and B. Srinivasan, "Growth, spectral, thermal, electrical, mechanical and nonlinear optical properties of organic single crystal 4-Amino-(1-methylphenyl) pyridinium bromide," Optik, vol. 157, pp. 774-786, Mar. 2018, https://doi.org/10.1016/j.ijleo.2017.11.141.
- [28] E. M. Onitsch, "The present status of testing the hardness of materials," Mikroskopie, vol. 95, no. 15, pp. 12-14, 1956.
- [29] Hanneman M, "Indentation size effect and microhardness study," Metall Manchu, vol. 23, no. 135-139, 1941.
- [30] P. P. Vinaya, A. N. Prabhu, K. Subrahmanya Bhat, and V. Upadhyaya, "Design, growth and characterization of D-π-A-π-D based efficient nonlinear optical single crystal for optical device

- applications," J. Phys. Chem. Solid., vol. 123, pp. 300-310, Dec. 2018, https://doi.org/10.1016/j.jpcs.2018.08.014.
- [31] M. S. Kajamuhideen, K. Sethuraman, P. Sasikumar, and H. Shakila, "Investigation on growth, physico-chemical properties, density functional theory and anti-microbial studies of a new organic acentric NLO crystal: Bis (2-aminobenzimidazolium) phthalate," Mat. Sci. Eng. B, vol. 240, pp. 106-115, Jan. 2019, https://doi.org/10.1016/j.mseb.2019.01.012.
- [32] P. P. Vinaya, A. N. Prabhu, K. S. Bhat, and V. Upadhyaya, "Synthesis, growth and characterization of a long-chain πconjugation based methoxy chalcone derivative single crystal; a third order nonlinear optical material for optical limiting applications," Optic. Mater., vol. 89, pp. 419-429, Mar. 2019, https://doi.org/10.1016/j.optmat.2019.01.061.
- [33] P. Karuppasamy, T. Kamalesh, V. Mohankumar, et al., "Synthesis, growth, structural, optical, thermal, laser damage threshold and computational perspectives of 4-nitrophenol 4aminobenzoic acid monohydrate (4NPABA) single crystal," J. Mol. Struct., vol. 1176, pp. 254–265, Jan. 2019, https://doi.org/ 10.1016/j.molstruc.2018.08.074.
- [34] S. K. Kurtz and T. T. Perry, "A Powder Technique for the Evaluation of Nonlinear Optical Materials," J. Appl. Phys., vol. 39, no. 8, pp. 3798-3813, Jul. 1968, https://doi.org/10.1063/1.1656857.
- [35] P. Prabukanthan, R. Lakshmi, G. Harichandran, and C. S. Kumar, "Synthesis, structural, optical and thermal properties of Nmethyl-N-aryl benzamide organic single crystals grown by a slow evaporation technique," J. Mol. Struct., vol. 1156, pp. 62-73, Mar. 2018, https://doi.org/10.1016/j.molstruc.2017.11.075.
- [36] T. D. Rani, M. Rajkumar, and A. Chandramohan, "Synthesis, crystal structure, thermal, mechanical and laser damage threshold studies of an NLO active organic molecular adduct: 4-Acetylpyridine:4-aminobenzoicacid," Mater. Lett., vol. 222, pp. 118-121, Jul. 2018, https://doi.org/10.1016/j.matlet.2018.
- [37] A. Jagadesan, N. Sivakumar, R. M Kumar, G. Chakkaravarthi, and S. Ariunan, "Synthesis, crystal structure, growth and characterization of an optical organic material: 4-Aminopyridinium Trichloro acetate single crystal," Opt. Mater., vol. 84, pp. 864–869, Oct. 2018, https://doi.org/10.1016/j. optmat.2018.08.025.
- [38] B. K. Revathi, D. R. Jonathan, S. Sathya, and G. Usha, "Crystal growth and characterization of new nonlinear optical piperidine derivative: (4-hydroxypiperidin-1-yl)(4-methylphenyl) methanone," J. Mol. Struct., vol. 1154, pp. 496-503, Feb. 2018, https://doi.org/10.1016/j.molstruc.2017.10.043.
- [39] C. S. Suchand Sandeep, A. K. Samal, T. Pradeep, and R. Philip, "Optical limiting properties of Te and Ag2Te nanowires," Chem. Phys. Lett., vol. 485, no. 4-6, pp. 326-330, Jan. 2010, https:// doi.org/10.1016/j.cplett.2009.12.065.
- [40] E. Mathew, V. V. Salian, I. H. Joe, and B. Narayana, "Third-order nonlinear optical studies of two novel chalcone derivatives using Z-scan technique and DFT method," Optics Laser Technol., vol. 120, p. 105697, Dec. 2019, https://doi.org/10.1016/j.optlastec. 2019.105697.
- [41] M. C. Sreenath, I. H. Joe, and V. K. Rastogi, "Third-order optical nonlinearities of 1,5-Diaminoanthraquinone for optical limiting application," Optics Laser Technol., vol. 108, pp. 218-234, Dec. 2018, https://doi.org/10.1016/j.optlastec.2018.06.056.
- [42] B. Chandrakantha, A. M. Isloor, R. Philip, M. Mohesh, P. Shetty, and A. M. Vijesh, "Synthesis and nonlinear optical

- characterization of new 1,3,4-oxadiazoles," Bull. Mater. Sci., vol. 34, no. 4, pp. 887-891, Jul. 2011, https://doi.org/10.1007/ s12034-011-0210-5.
- [43] A. Jayashree, B. Narayana, S. M. Kumar, K. R. Raghi, B. K. Sarojini, and T. K. M. Kumar, "Synthesis, X-ray crystal structure,

Hirshfeld surface analysis, DFT, MESP and molecular docking studies of 2-(4-bromophenyl)-1-(3-fluoro-4-methylphenyl)-4,5diphenyl-1H-imidazole," Chem. Data Collections, vol. 21, p. 100237, Jun. 2019, https://doi.org/10.1016/j.cdc.2019. 100237.